Parathyroid hormone is essential for normal fetal bone formation

Dengshun Miao,[1] Bin He,[2] Andrew C. Karaplis,[2] and David Goltzman[1]

[1]Calcium Research Laboratory, McGill University Health Centre, and Department of Medicine, McGill University, Montreal, Quebec, Canada
[2]Lady Davis Research Institute, Sir Mortimer B. Davis Jewish General Hospital, and Department of Medicine, McGill University, Montreal, Quebec, Canada

Address correspondence to: David Goltzman, Calcium Research Laboratory, Room H4.67, Royal Victoria Hospital, 687 Pine Avenue West, Montreal, Quebec H3A 1A1, Canada.
Phone: (514) 843-1632; Fax: (514) 843-1712; E-mail: david.goltzman@mcgill.ca.

Dengshun Miao and Bin He contributed equally to this work.

Received for publication November 26, 2001, and accepted in revised form March 18, 2002.

Parathyroid hormone (PTH) is a potent pharmacologic inducer of new bone formation, but no physiologic anabolic effect of PTH on adult bone has been described. We investigated the role of PTH in fetal skeletal development by comparing newborn mice lacking either PTH, PTH-related peptide (PTHrP), or both peptides. PTH-deficient mice were dysmorphic but viable, whereas mice lacking PTHrP died at birth with dyschondroplasia. PTH-deficient mice uniquely demonstrated diminished cartilage matrix mineralization, decreased neovascularization with reduced expression of angiopoietin-1, and reduced metaphyseal osteoblasts and trabecular bone. Compound mutants displayed the combined cartilaginous and osseous defects of both single mutants. These results indicate that coordinated action of both PTH and PTHrP are required to achieve normal fetal skeletal morphogenesis, and they demonstrate an essential function for PTH at the cartilage-bone interface. The effect of PTH on fetal osteoblasts may be relevant to its postnatal anabolic effects on trabecular bone.

J. Clin. Invest. **109**:1173–1182 (2002). DOI:10.1172/JCI200214817.

Introduction

Endogenous parathyroid hormone (PTH) functions to maintain normal extracellular calcium levels in the adult in part by enhancing osteoclastic bone resorption and liberating calcium from the adult skeleton. In contrast, exogenous PTH has been shown to exert significant skeletal anabolic effects in the adult when administered intermittently as a pharmacologic agent (1–4). No physiologic role for PTH on increasing bone formation has yet been demonstrated, and its role in fetal skeletal development is unknown. In contrast, PTH-related peptide (PTHrP) is known to play a critical and nonredundant role in fetal endochondral bone formation. Endochondral bone formation, in which bone is generated within a cartilage primordium, is a critical component of vertebrate skeletal development (5). Cells committed to the chondrogenic lineage progress through stages of proliferation, differentiation, hypertrophy, and apoptosis. Vascular invasion and degradation of calcified cartilage matrix then occurs, followed by secretion of trabecular bone matrix by invading osteoblasts. This complex process requires the coordinated activity of growth factors, hormones, proteases, and matrix molecules. Targeted disruption of the *PTHrP* gene results in lethal dyschondroplasia, caused mainly by a reduction of chondrocyte proliferation in the epiphyseal growth plate (6) and accelerated maturation of chondrocytes to hypertrophy (7). Both PTH and PTHrP interact at a common G protein–linked receptor termed the type I PTH/PTHrP receptor (PTHR). Ablation of the PTHR has been reported to simulate the effect of PTHrP ablation on chondrocyte differentiation (although more slowly) and to delay cartilage matrix mineral deposition, decrease vascular invasion of cartilage, and reduce trabecular bone formation in the primary spongiosa, alterations not seen after PTHrP ablation (8). These alterations were apparently partially alleviated when both PTHrP and the receptor were deficient. The mechanism for these effects, however, remained unclear.

To assess the role of PTH in modulating skeletal development in the fetus and any potential interaction of PTH and PTHrP, we analyzed tissues of newborn mice homozygous for targeted ablation of the genes encoding PTH ($PTH^{-/-}$), PTHrP ($PTHrP^{-/-}$), and both PTH and PTHrP ($PTH^{-/-}$, $PTHrP^{-/-}$) and compared these to each other and to wild-type mice.

Methods

Mouse models. Mice carrying a disrupted *PTH* gene ($PTH^{-/-}$ mice) or a disrupted *PTHrP* gene ($PTHrP^{-/-}$ mice) were derived by homologous recombination in embryonic stem cells (9, 10). To generate $PTH^{-/-}$ mice, the murine *PTH* gene (GenBank accession numbers AF066074 and AF066075), which has an organizational structure and exon-intron boundaries identical to the human, bovine, and rat *PTH* genes (11), was introduced into the pPNT vector (12), replacing the entire coding

sequence of mature PTH on exon 3 (11) with a neomycin resistance gene. The vector was electroporated into D3 embryonic stem cells, and following G418 selection, clones were injected into BALB/C blastocytes. Chimeric male mice were mated to C57BL/6J females, and following germline transmission, mice were bred to homozygosity for the null *PTH* allele. To obtain double knockout mice that are disrupted for both the *PTH* and the *PTHrP* genes ($PTH^{-/-}$, $PTHrP^{-/-}$ mice), we mated *PTH* homozygous mice and *PTHrP* heterozygous mice, males and females, on a C57BL/6J background. Genomic DNA was isolated from tail clips for genotyping of mice by standard methods described previously (10). Wild-type and mutant *PTH* alleles were detected using a 0.2-kb HindIII/XhoI genomic DNA fragment as probe following digestion of tail tip genomic DNA with BamHI. For detecting *PTHrP* wild-type and mutant alleles, a 0.62-kb SacI/XhoI genomic fragment was used following digestion of tail tip genomic DNA with PvuII. All animal studies were conducted in accordance with principles and procedures dictated by the highest standards of humane animal care.

Skeletal preparations and histology. Newborn mice were sacrificed in a CO_2 chamber. After sacrifice, for skeletal preparations, newborn mice were eviscerated, fixed with 95% ethanol overnight, and stained with Alcian blue for cartilage and with alizarin red for calcified tissue as described previously (13). For histologic analysis, femurs and tibiae were fixed and cut into sections as described previously (14). The sections were stained with hematoxylin and eosin (H&E) or immunostained. Apoptotic cells were detected as described below. Undecalcified right femurs and tibiae were embedded in LR White acrylic resin (London Resin Co., London, United Kingdom), and 1-μm sections were cut on an ultramicrotome. Sections were stained for mineral with the von Kossa procedure and counterstained with toluidine blue.

Immunohistochemistry. Paraffin-embedded sections of decalcified skeleton and of parathyroid glands were stained immunohistochemically for PTH, PTHrP, calcium-sensing receptor (CaSR), proliferating cell nuclear antigen (PCNA), type X collagen, VEGF, angiopoietin-1 (Ang-1), and endothelial nitric oxide synthase (eNOS) using the avidin-biotin-peroxidase complex (ABC) technique as described previously (15).

The following antisera were used: goat anti-serum raised by us against PTH[1-34]; mouse anti-CaSR monoclonal antibody (15); rabbit anti-serum against PTHrP[1-34] (6); mouse anti-PCNA monoclonal antibody (Medicorp Inc., Montreal, Canada); rabbit antiserum against type X collagen (a generous gift from A.R. Poole, Shriners Hospital, Montreal, Canada); goat antiserum against VEGF and Ang-1 (Santa Cruz Biotechnology Inc., Santa Cruz, California, USA), and mouse anti-eNOS monoclonal antibody (Zymed Laboratories Inc., San Francisco, California, USA).

Detection of apoptotic cells. Dewaxed paraffin-embedded sections were stained with an in situ cell death detection kit (Boehringer Mannheim, Laval, Quebec, Canada) according to the manufacturer's instructions. Briefly, following treatment with 3 μg/ml of proteinase K for 20 minutes at room temperature, the sections were incubated with a TUNEL reaction mixture for 60 minutes at 37°C. Sections were then incubated with Converter-AP (Sigma, St. Louis, Missouri, USA) for 30 minutes at 37°C, and alkaline phosphatase was visualized after 10–15 minutes of treatment with Fast Red TR/Naphthol AS-MX phosphate (Sigma, St. Louis, Missouri, USA) containing 1 mM levamisole as an endogenous alkaline phosphatase inhibitor. Sections were counterstained with methyl green and mounted with Kaiser's glycerol jelly.

Computer-assisted image analysis. After H&E staining or immunostaining of sections from three each of the wild-type; $PTH^{-/-}$; $PTHrP^{-/-}$; and $PTH^{-/-}$, $PTHrP^{-/-}$ mice, images of fields (shown in Figures 2–6) were photographed with a Sony digital camera. Images of micrographs from single sections were digitally recorded using a rectangular template, and recordings were processed using Northern Eclipse image analysis software, version 5.0 (Empix Imaging Inc., Mississauga, Ontario, Canada) (15). For determining the area or number of immunoreactions and the area of mineralized matrix in stained bone sections, thresholds were set using green and red channels. The thresholds were determined as described previously (15, 16).

Statistical analysis. Data from image analysis are presented as mean ± SEM. Statistical comparisons were made using a two-way ANOVA, with a probability of less than 0.05 being considered significant.

Results

Effects of gene deletion on PTH and PTHrP production. Using Southern blot analysis of genomic DNA, we first identified mice lacking expression of PTH and/or PTHrP amongst the newborn offspring. The expected bands of 6.2 kb and 1.0 kb were observed for wild-type *PTH* and wild-type *PTHrP* alleles, respectively, and expected bands of 4.0 kb and 1.8 kb were observed for the targeted *PTH* (9) and *PTHrP* alleles (10), respectively (Figure 1a).

We next investigated the effect of *PTH* and *PTHrP* gene deletion on the size and function of the parathyroid glands (Figure 1, b–d). Parathyroid glands were greatly enlarged in the $PTH^{-/-}$ mice and were moderately enlarged in $PTHrP^{-/-}$ mice, but were most dramatically enlarged in the $PTH^{-/-}$, $PTHrP^{-/-}$ mice compared with the wild-type mice (Figure 1b). In wild-type mice, the parathyroid glands expressed both PTH and the CaSR, which detects extracellular fluid calcium levels (17) (Figure 1, c and d). PTH expression was absent in the parathyroids of the two PTH-deficient mouse models but was detectable in the $PTHrP^{-/-}$ mice (Figure 1c). Enlarged parathyroid glands were therefore present in all three models of targeted gene ablation and expressed substantial CaSR, a moiety reported to be functional in fetal life (18). This supports the view that ambient hypocalcemia existed in the mutants and

stimulated parathyroid growth. Indeed, in view of the fact that PTHrP is required for maintaining the transplacental calcium flux needed for fetal calcium homeostasis, elevated blood PTH levels have previously been postulated to be increased in *PTHrP*$^{-/-}$ mice (8).

We next examined PTHrP production in the mutants (Figure 1e). PTHrP expression in the chondrocytes of the growth plates was equivalent in the *PTH*$^{-/-}$ mice and wild-type littermates but was not detected in the two *PTHrP*$^{-/-}$ mouse models (Figure 1e). The absence of both PTHrP and PTH in the compound mutant led to the greatest enlargement of the parathyroid glands (Figure 1, b–d), consistent with the absence of two calcium-regulating entities (19).

Skeletal phenotypes and alterations of the cartilaginous growth plate. In *PTH*$^{-/-}$ mice, compared with wild-type mice, the skull was abnormally formed and mineralization of the bones of the skull was enhanced. The vertebral column was also abnormal, with evidence of smaller vertebral bodies, and mineralized metacarpal and metatarsal bones were shorter (Figure 2, a versus b). Although the *PTH*$^{-/-}$ mice were viable, *PTHrP*$^{-/-}$ and compound mutant mice died at birth, with skeletal malformations including short-limbed dwarfism that were most severe in the compound mutants. The whole skeleton of the compound mutant mouse was smaller than that of the *PTH*$^{-/-}$ mouse and the *PTHrP*$^{-/-}$ mouse (Figure 2, d versus b or c), and all elements of the axial and appendicular skeletons were more dramatically reduced in size. In both the *PTHrP*$^{-/-}$, *PTH*$^{-/-}$ mice and *PTHrP*$^{-/-}$ mice, less cartilage staining relative to calcified skeletal staining was observed than was seen in the wild-type mice (Figure 2, c and d versus a).

From H&E-stained sections (Figure 2, e–h), we could identify regions of proliferating chondrocytes, hypertrophic chondrocytes, and bone tissue in the long bones of all models. The overall lengths of tibiae (Figure 2i) and of proliferating zones (Figure 2j) were normal in the *PTH*$^{-/-}$ mice, reduced in the *PTHrP*$^{-/-}$ mice compared with wild-type mice, and reduced even further in the

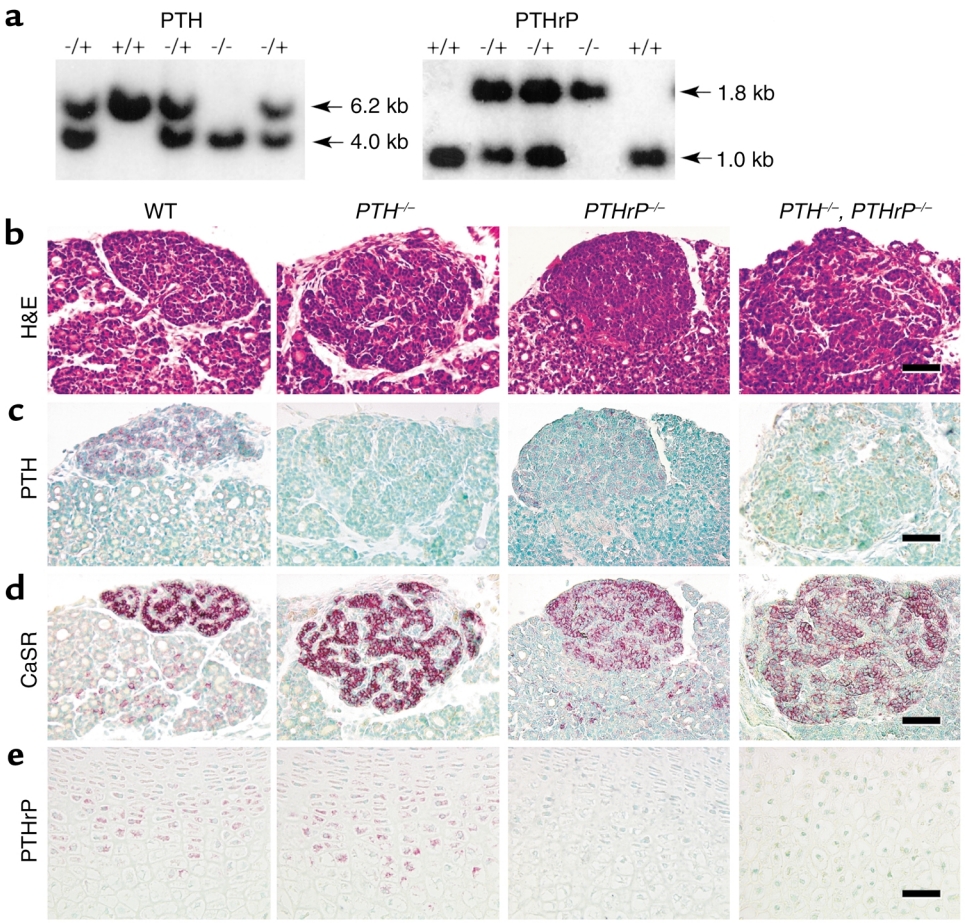

Figure 1
Genotyping of mice and examination of the expression of PTH and PTHrP. (**a**) Analysis of genomic DNA isolated from pups born of *PTH*$^{-/-}$ and *PTHrP*$^{+/-}$ matings. For Southern blots, purified DNA was digested with BamHI for PTH and with PvuII for PTHrP. The mutated *PTH* allele (4.0 kb) and *PTHrP* allele (1.8 kb) are distinguished from the wild-type PTH (6.2 kb) and PTHrP (1.0 kb) alleles using the probes described in Methods. (**b**–**d**) Thyroid and parathyroid gland paraffin-embedded sections from wild-type (WT), *PTH*$^{-/-}$; *PTHrP*$^{-/-}$; and *PTH*$^{-/-}$, *PTHrP*$^{-/-}$ mice were stained with H&E (**b**) and immunostained for PTH (**c**) and CaSR (**d**). Paraffin-embedded sections of tibial epiphyseal cartilage were immunostained for PTHrP (**e**). Scale bars represent 50 μm.

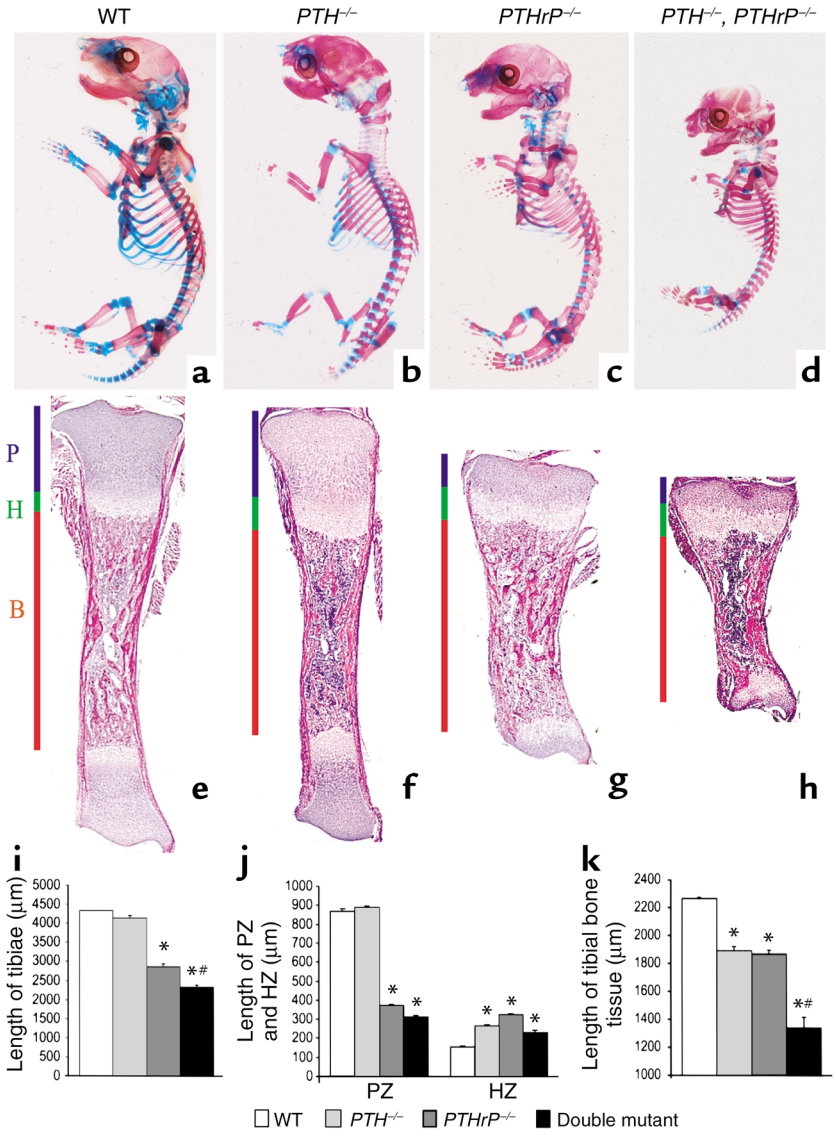

Figure 2
Skeletal phenotypes and tibial histology of mutant mice. The skeletons from newborn wild-type; *PTH*$^{-/-}$; *PTHrP*$^{-/-}$; and *PTH*$^{-/-}$, *PTHrP*$^{-/-}$ mice were stained with Alcian blue (for cartilage) and alizarin red (for calcified tissue) as described in Methods. (**a**–**d**) Whole mount of skeletons. (**e**–**h**) Sections of tibiae from wild-type; *PTH*$^{-/-}$; *PTHrP*$^{-/-}$; and *PTH*$^{-/-}$, *PTHrP*$^{-/-}$ mice stained with H&E and photographed at a magnification of 25. P, proliferating zone. H, hypertrophic zone. B, bone tissue. (**i** and **j**) The length of whole tibiae, of the proliferating zones (PZs), and of the hypertrophic zones (HZs) of the growth plates were measured from three each of the wild-type; *PTH*$^{-/-}$; *PTHrP*$^{-/-}$; and *PTH*$^{-/-}$, *PTHrP*$^{-/-}$ mice and are presented as mean ± SEM, respectively. (**k**) The length of tibial bone tissue is presented as the mean ± SEM of three determinations. **P* < 0.05, mutant mice relative to wild-type mice. #*P* < 0.05 in compound mutant mice relative to *PTH*$^{-/-}$ or *PTHrP*$^{-/-}$ mice.

PTH$^{-/-}$, *PTHrP*$^{-/-}$ mice (Figure 2, i and j, respectively). The hypertrophic zone was enlarged in all three models compared with the wild-type mice (Figure 2j). The ratio of hypertrophic zone to proliferating zone was high in the *PTHrP*$^{-/-}$ mice and greatest in the *PTH*$^{-/-}$, *PTHrP*$^{-/-}$ mice.

Proliferation of chondrocytes was not altered in the *PTH*$^{-/-}$ mice, but was dramatically decreased in the two PTHrP-deficient mouse models compared with wild-type mice (Figure 3, c and d versus a, and Figure 3m). The number of apoptotic chondrocytes was increased fivefold in the two PTHrP-deficient mice compared with wild-type mice (Figure 3, g and h versus e, and Figure 3m), consistent with previous reports (20, 21), but was not changed in the *PTH*$^{-/-}$ mice (Figure 3, f versus e, and Figure 3m).

The deposition of type X collagen in the matrix of the hypertrophic zone was slightly enhanced in the *PTH*$^{-/-}$ mice (Figure 3, j versus i, and Figure 3n) but was substantially increased in both the *PTHrP*$^{-/-}$ mice and the *PTH*$^{-/-}$, *PTHrP*$^{-/-}$ mice, in keeping with accelerated rates of differentiation and enlargement of the hypertrophic zones (Figure 3, k and l versus i, and Figure 3n).

Alterations of the chondro-osseous junction. Mineralization of cartilage matrix was enhanced in the *PTHrP*$^{-/-}$ mice (Figure 4, c versus a, and Figure 4m), but was reduced in the *PTH*$^{-/-}$ mice (Figure 4, b versus a, and Figure 4m) and in the *PTH*$^{-/-}$, *PTHrP*$^{-/-}$ mice (Figure 4, d versus a, and Figure 4m).

In view of the fact that mRNA encoding VEGF is expressed by hypertrophic chondrocytes in the epiphyseal growth plate and VEGF-dependent blood vessels are essential for coupling cartilage resorption with bone formation (22), we assessed the presence of VEGF by immunostaining. The results confirmed that VEGF was indeed expressed in chondrocytes of the hypertrophic zone in the wild-type mice (Figure 4e) and was also seen in this zone in each of the mutant models (Figure 4, f–h). The VEGF-positive area was significantly increased in all three animal models compared with the wild-type mice (Figure 4n).

Despite abundant VEGF expression, however, vascular invasion in the growth plate was reduced in both the *PTH*$^{-/-}$ mice and the compound mutants (Figure 2, f and h versus e) but not in the *PTHrP*$^{-/-}$ animals (Figure 2, g versus e). Ang-1 is an angiogenic regulator that recruits and interacts with periendothelial support cells and is required for blood vessel integrity (23). Ang-1 was detected in chondrocytes in the growth plate of wild-type mice (Figure 4i) and was increased in maturing and hypertrophic chondrocytes of *PTHrP*$^{-/-}$ mice (Figure 4, k and o), but was diminished in both *PTH*$^{-/-}$ models (Figure 4, j, l, and o). Consequently, reduced Ang-1 levels correlated with the decreased vascular invasion.

Overall, PTH deficiency in the two *PTH*$^{-/-}$ models was associated with reductions in both cartilage matrix mineralization and vascular invasion. The opposite was observed in the *PTHrP*$^{-/-}$ mice, possibly reflecting elevated circulating PTH levels in that model.

Effects on cortical and trabecular bone. The length of bone tissue was reduced in the long bones of *PTH*$^{-/-}$ mice and *PTHrP*$^{-/-}$ mice, and was reduced even more dramatically in the *PTH*$^{-/-}$, *PTHrP*$^{-/-}$ mice compared with the wild-type mice (Figure 2, f versus e; g versus e; and h versus e, respectively; and Figure 2k). The cortical thickness of long bones was increased in all three mutant models compared with that in wild-type mice (Figure 5, a–d and m). In contrast, trabecular bone volume, although somewhat increased in the *PTHrP*$^{-/-}$ mice, was diminished in the *PTH*$^{-/-}$ mice, and was even more dramatically diminished in the *PTH*$^{-/-}$, *PTHrP*$^{-/-}$ mice compared with the wild-type mice (Figure 5, a–d and n).

Decreased osteoblast numbers were found in the primary spongiosa of the *PTH*$^{-/-}$ mice and the *PTH*$^{-/-}$, *PTHrP*$^{-/-}$ mice, whereas osteoblast numbers were increased in the primary spongiosa of the *PTHrP*$^{-/-}$ mice, possibly reflecting secondary hyperparathyroidism (Figure 5, e–h and Figure 5o). In the endosteum, changes in osteoblast numbers were similar to those in the primary spongiosa (Figure 5, i–l). In contrast, periosteal cells were not altered significantly in any of the three models compared with wild-type mice (Figure 5, i–l). Consequently, reduced osteoblast numbers in the primary spongiosa

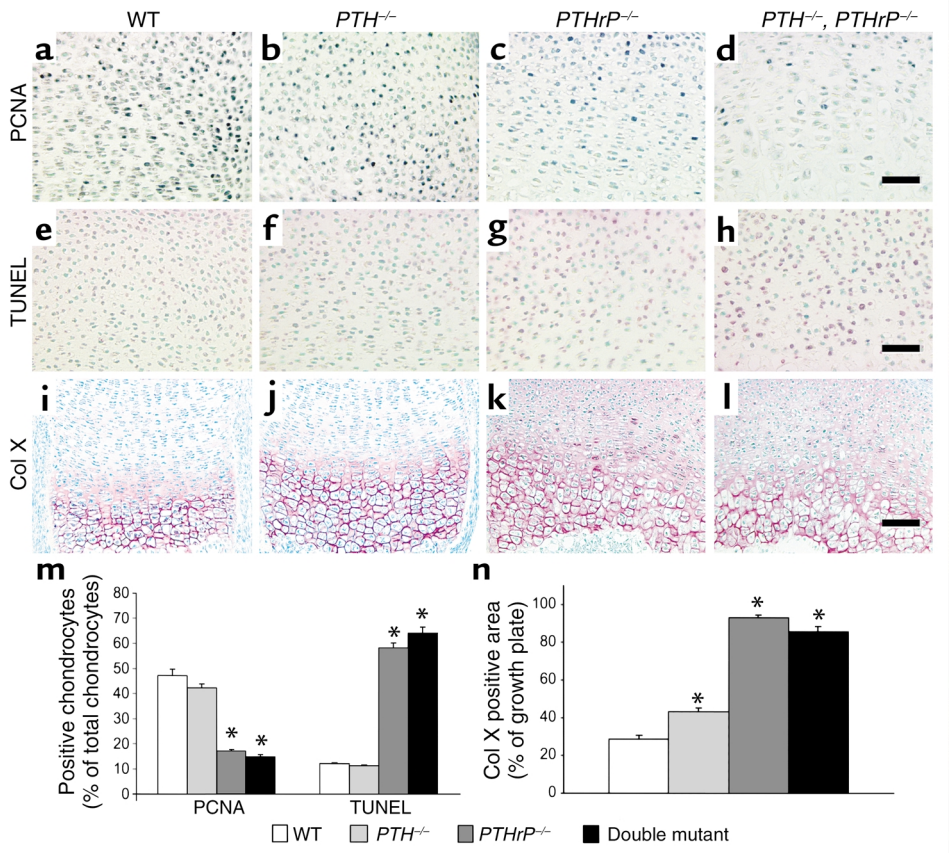

Figure 3

Assessment of indices of chondrocyte proliferation, apoptosis, and differentiation. (**a**–**d**) Paraffin-embedded sections of tibiae from wild-type; *PTH*$^{-/-}$; *PTHrP*$^{-/-}$; and *PTH*$^{-/-}$, *PTHrP*$^{-/-}$ mice were immunostained for PCNA as described in Methods. (**e**–**h**) Sections were stained for apoptosis using TUNEL. (**i**–**l**) Sections were immunostained for type X collagen (Col X). Scale bars in **d**, **h**, and **l** represent 50 μm. (**m**) The numbers of PCNA-positive chondrocytes, of TUNEL-positive chondrocytes, and of total chondrocytes per field were determined by image analysis; the PCNA-positive and TUNEL-positive percentages of total chondrocytes counted are presented as the mean ± SEM of triplicate determinations. (**n**) Immunostaining for type X collagen was performed as described in Methods, and the immunopositive area as a percentage of the growth plate field was determined. The percent-positive area is presented as mean ± SEM of triplicate determinations. *$P < 0.05$ in the mutant mice relative to the wild-type mice.

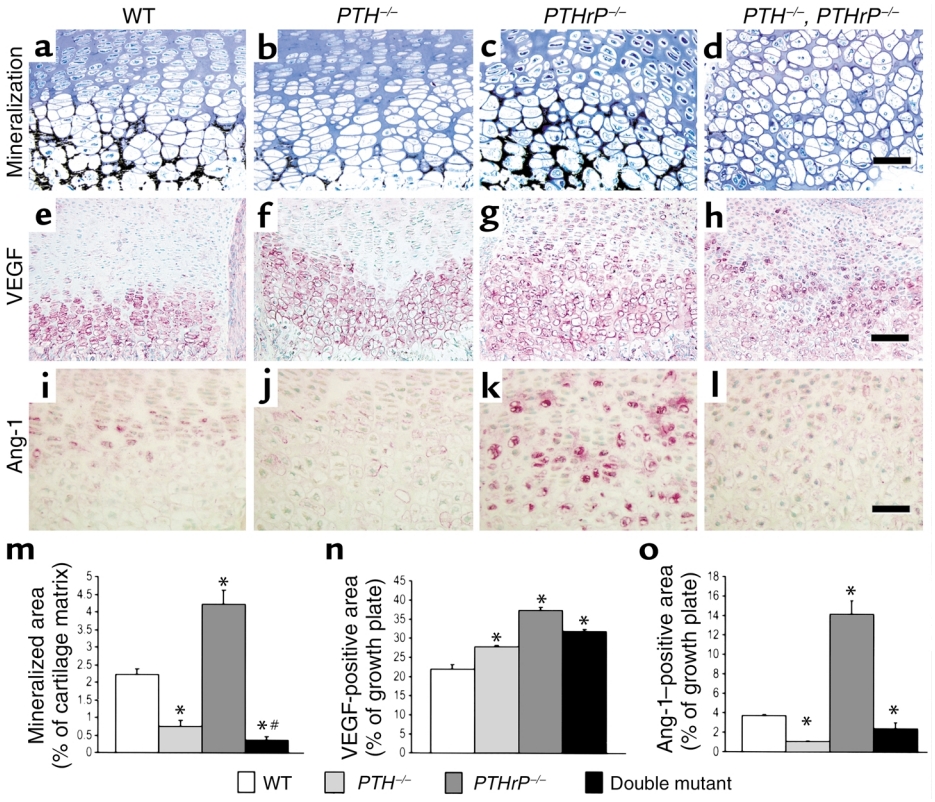

Figure 4
Examination of cartilage matrix mineralization and angiogenesis regulators. (**a**–**d**) Undecalcified sections of femurs from wild-type; *PTH*$^{-/-}$; *PTHrP*$^{-/-}$; and *PTH*$^{-/-}$, *PTHrP*$^{-/-}$ mice were stained with von Kossa stain as described in Methods. (**e**–**h**) Paraffin-embedded sections were immunostained for VEGF as described in Methods. (**i**–**l**) Sections were immunostained for Ang-1. Scale bars in **d**, **h**, and **l** represent 50 µm. (**m**) The mineralized area as a percent of the cartilage matrix per field was determined by image analysis as described in Methods and is presented as the mean ± SEM of triplicate determinations. (**n**) The VEGF-immunopositive area as a percentage of the growth plate field was determined by image analysis and is presented as mean ± SEM of triplicate determinations. (**o**) The immunopositive area of Ang-1 as a percentage of the growth plate field was determined by image analysis and is presented as the mean ± SEM of triplicate determinations. **P* < 0.05, mutant mice relative to wild-type mice. #*P* < 0.05, compound mutant mice relative to *PTH*$^{-/-}$ mice or *PTHrP*$^{-/-}$ mice.

appeared to account for the reduced trabecular bone volume in the two *PTH*$^{-/-}$ models, and PTH appears to be essential for optimal osteoblast production in this region of fetal trabecular bone.

Nitric oxide has been implicated in the local regulation of skeletal metabolism, and mice with ablation of the gene encoding eNOS develop osteoblast defects and reduced bone formation (24). We therefore examined the expression of eNOS in chondrocytes and osteoblasts from the gene knockout animals. In wild-type mice, eNOS was expressed at high levels in osteoblasts in the metaphysis and was also detected in some hypertrophic chondrocytes. The expression of this enzyme in both chondrocytes and metaphyseal osteoblasts was enhanced in the *PTHrP*$^{-/-}$ mice, but was reduced in both the *PTH*$^{-/-}$ mice and the *PTH*$^{-/-}$, *PTHrP*$^{-/-}$ mice (Figure 6, a–d and m). Whether this reduction is a consequence of PTH deficiency that contributes to diminished osteoblast production or is simply a reflection of decreased osteoblast numbers remains to be determined.

We found increased levels of apoptosis in osteoblasts and osteocytes in the endosteum of all three models compared with those in wild-type mice (Figure 6, e–h and n). Consequently, both PTH and PTHrP appear to protect osteoblasts from apoptosis.

Using histochemical staining for tartrate-resistant acid phosphatase (TRAP) (Figure 6, i–l) and subsequent image analysis, we found that the number (Figure 6o) and size (Figure 6p) of osteoclasts were decreased in all three mutant models compared with those in wild-type mice, but were most dramatically reduced in the compound homozygous mice. Consequently, diminished bone resorption in the absence of either PTH or PTHrP appears to explain the increased cortical thickness observed in all three models.

Discussion

Our studies show that both PTH and PTHrP are necessary for normal fetal endochondral bone formation and that they appear mainly to regulate discrete regions of the growth plate in a complementary fashion. PTH is expressed only in the parathyroid glands, and its synthesis and secretion is tightly regulated by ambient calcium through CaSR (17). Its access to the skeleton is via the circulation, and following PTH

ablation, the alterations we have identified at the chondro-osseous junction are consistent with its entry to the developing skeleton via the microvasculature in this region. The reduced Ang-1 levels observed in the *PTH*$^{-/-}$ animals may contribute to poorly developed capillary invasion (23) and consequently lead to reduced cartilage matrix mineralization and diminished entry of precursors for cells of the osteoblastic and chondroclastic lineages.

Thus, diminished resorption of terminally differentiated chondrocytes is the most likely cause of the slightly expanded hypertrophic zone observed in *PTH*$^{-/-}$ mice that was evidenced by the pattern of type X collagen and VEGF expression. This enlarged hypertrophic zone accounted for the modest increase in the overall size of the growth plate. Therefore, PTH seems essential for normal cartilage remodeling. In addition, the reduced osteoblast production in the absence of PTH led to a poorly developed primary spongiosa and ultimately to reduced trabecular bone volume. Whether this effect is in part mediated by nitric oxide production remains to be determined (24). Nevertheless, this reduction resulted in a decrease in the length of bone tissue per se, although the overall length of the tibia was almost normal in the *PTH*$^{-/-}$ mice due to the modest increase in the size of the cartilaginous growth plate.

It has previously been reported that *PTHrP*$^{-/-}$ mice have reduced capacity to maintain normal placental calcium transport and therefore develop hypocalcemia (18, 19). Our studies show that secondary enlargement

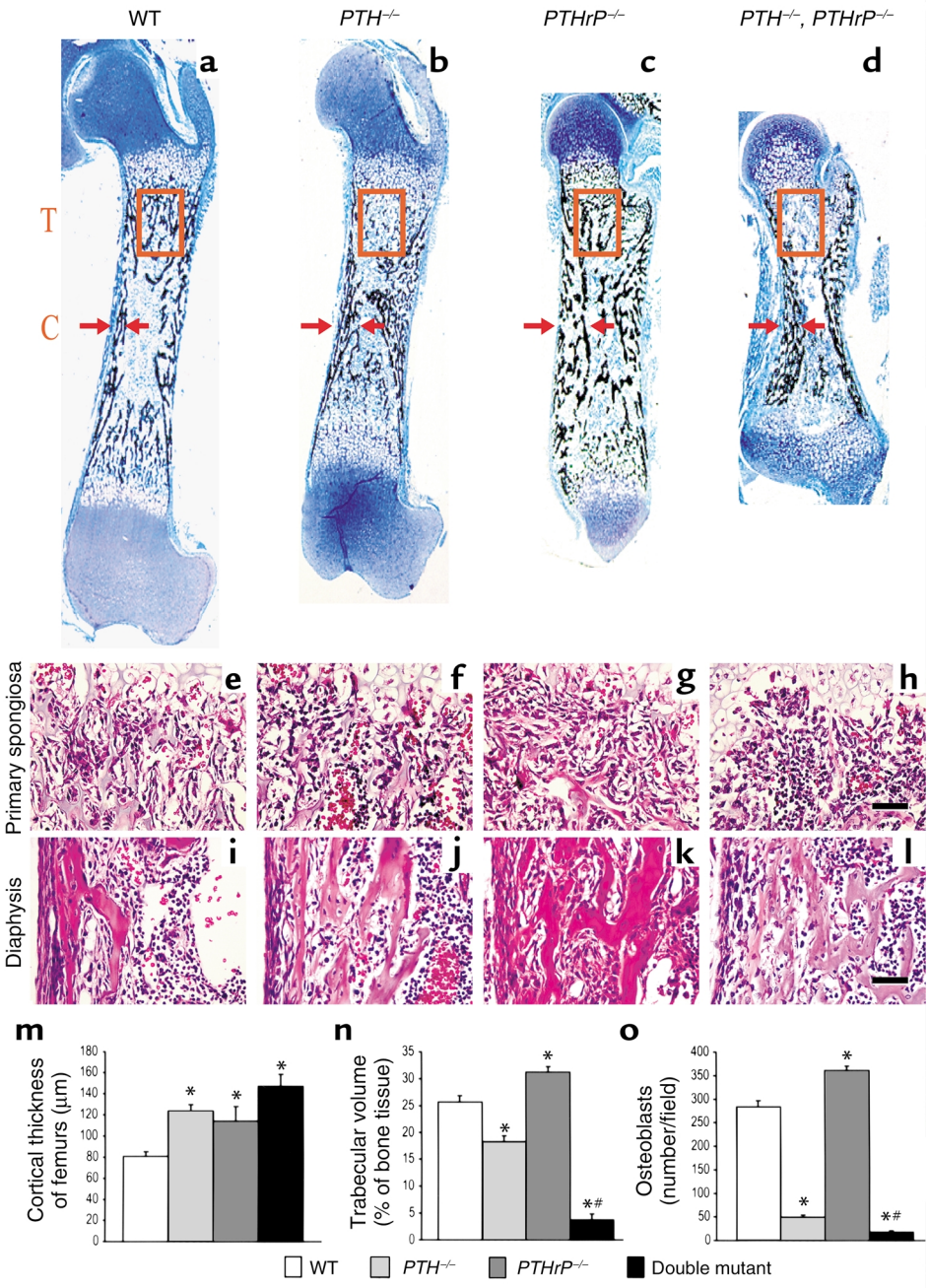

Figure 5
Quantitation of bone parameters. (**a**–**d**) Undecalcified sections of femurs stained with von Kossa stain as described in Methods and photographed at a magnification of 25. T, trabecular bone (red square). C, cortical bone (arrows). (**e**–**h**) Primary spongiosa from wild-type; *PTH*$^{-/-}$; *PTHrP*$^{-/-}$; and *PTH*$^{-/-}$, *PTHrP*$^{-/-}$ mice stained with H&E. (**i**–**l**) Diaphyseal region from wild-type and mutant mice stained with H&E. (**m** and **n**) The cortical thickness and trabecular bone volume were measured from three each of the wild-type; *PTH*$^{-/-}$; *PTHrP*$^{-/-}$; and *PTH*$^{-/-}$, *PTHrP*$^{-/-}$ mice and presented as mean ± SEM. (**o**) The number of osteoblasts per field were counted in triplicate in the primary spongiosa of H&E-stained femurs of the mice and presented as mean ± SEM. **P* < 0.05, mutant mice relative to wild-type mice. #*P* < 0.05, compound mutant mice relative to *PTH*$^{-/-}$ mice or *PTHrP*$^{-/-}$ mice.

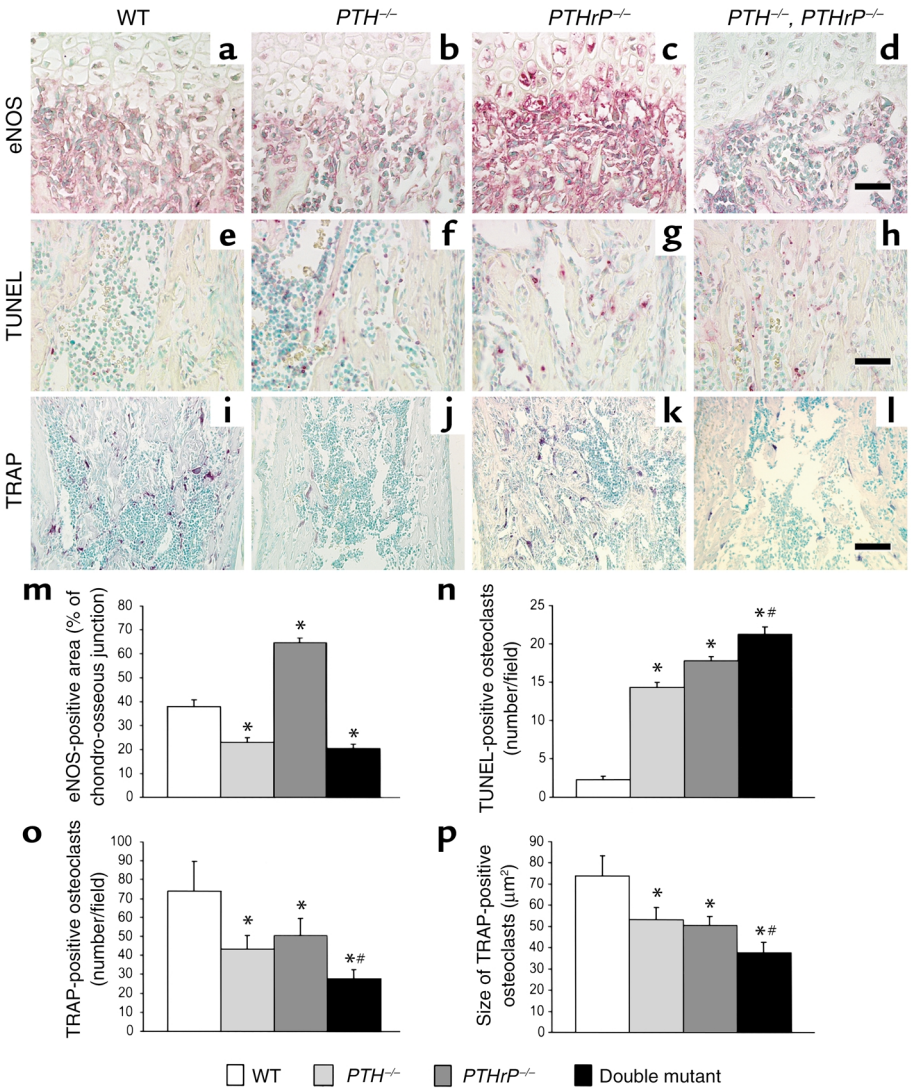

Figure 6
Histologic analysis of bone parameters. (**a**–**d**) The chondro-osseous junction of the femur from wild-type; *PTH*$^{-/-}$; *PTHrP*$^{-/-}$; and *PTH*$^{-/-}$, *PTHrP*$^{-/-}$ mice immunostained for eNOS. (**e**–**h**) TUNEL reaction to detect apoptotic osteoblasts and osteocytes, performed as described in Methods. (**i**–**l**) Sections stained histochemically for TRAP to detect osteoclasts. Scale bars in **d**, **h**, and **l**, represent 50 μm. (**m**) The eNOS-immunopositive area as a percentage of each field in the chondro-osseous junction was determined by image analysis as described in Methods and is presented as the mean ± SEM of triplicate determinations. (**n**) The numbers of apoptotic osteoblasts or osteocytes per field as determined by TUNEL assay were quantitated by image analysis and are presented as mean ± SEM of triplicate determinations. (**o**) The number of TRAP-positive osteoclasts per field was determined by image analysis. Data is presented as mean ± SEM. (**p**) The mean size of TRAP-positive osteoclasts was also determined in the same fields by image analysis and is presented as the mean ± SEM of triplicate determinations. **P* < 0.05 relative to the wild-type mice. #*P* < 0.05, *PTH*$^{-/-}$, *PTHrP*$^{-/-}$ mice relative to *PTHrP*$^{-/-}$ mice or *PTH*$^{-/-}$ mice.

of the parathyroid gland ensues (Figure 1, c and d). Increased PTH secretion by the enlarged glands may therefore lead to augmented Ang-1 levels and increases in capillary invasion, cartilage matrix mineralization, and osteoblast numbers in the primary spongiosa. These changes were indeed observed at the chondro-osseous junction in the *PTHrP*$^{-/-}$ mice but were not seen when the *PTH* gene was deleted from these mice. Consequently, among other actions, the predominant effect on the osteoblast in the primary spongiosa at this stage of development appeared to be related to PTH rather than PTHrP. Our studies therefore provide the first evidence that PTH has a physiologic role as an "anabolic agent" in bone.

PTHrP, but not PTH, is expressed in a wide array of cells and tissues including both proliferative and hypertrophic chondrocytes (6, 20). Consequently, PTHrP rather than PTH can exert autocrine/paracrine actions in the avascular cartilaginous growth plate where major consequences occur after PTHrP ablation (6, 10). The action on proliferating and differentiating chondrocytes specifically attributable to PTHrP may also reflect the earlier appearance of PTHrP than of PTH in embryogenesis and therefore

its more profound involvement in cartilage morphogenesis, which begins prior to the development of the parathyroid glands (embryonic day 11.5–12.5 versus day 14.5–15.5, respectively) (25).

Enlargement of the parathyroid glands was also observed in the PTH-ablated mice, a finding that is consistent with fetal hypocalcemia (19). Therefore, PTH per se plays a role in maintaining calcium homeostasis in the fetus. Nevertheless, no alteration in PTHrP expression was observed in cartilage of *PTH*$^{-/-}$ mice (Figure 1e). These observations therefore emphasize the insensitivity of PTHrP expression, at least in growth plate cartilage, to the ambient calcium concentration.

The different sites of production of these two peptides, their differential responses to ambient calcium, and their different modes of action, i.e., long range (endocrine) versus short range (paracrine/autocrine), may therefore largely contribute to the phenotypic characteristics we observed in the developing growth plate.

Although PTH deficiency in both *PTH*$^{-/-}$ mice and the compound mutant mice caused a decrease in osteoblast numbers in the primary spongiosa, this was not observed in periosteal bone. Differential effects of a constitutively active PTHR on metaphyseal versus periosteal osteoblasts have previously been described, and our findings are consistent with these observations (26). In the endosteum, apoptosis in cells of the osteoblast lineage was increased in association with ablation of both PTH and PTHrP. Previous studies in vitro and after administration of PTH pharmacologically in vivo in postnatal animals have emphasized the important role PTH plays in inhibiting apoptosis (27, 28). Our studies demonstrate a physiologic role for both PTH and PTHrP in inhibiting apoptosis in osteoblasts in the developing fetal skeleton.

Molecular genetic studies have now shown that congenital hypoparathyroidism may be caused by defects in a variety of genes (29). Reduced PTH secretion may be caused by rare mutations in the *PTH* gene and have been associated with both autosomal dominant (30) and recessive forms of familial isolated hypoparathyroidism (31, 32). Gain-of-function mutations in the *CaSR* gene also impair PTH secretion and have been more frequently reported in association with a mild variant of hypoparathyroidism known as autosomal dominant hypocalcemia (33). Impaired development of the parathyroid glands has also been described. Thus, autosomal recessive isolated hypoparathyroidism has been associated with mutations in glial cells missing B (GCMB), a transcription factor that is required for normal parathyroid gland embryogenesis (34). Genetic ablation of the corresponding gene in mice, *Gcm*$_2$, also caused hypocalcemia, but the presence of normal circulating PTH concentrations in these animals led to the observation that the thymus might be an additional source of PTH (35). Although calcium and PTH levels are generally well documented in these cases of isolated congenital hypoparathyroidism, no detailed description of the neonatal hypoparathyroid skeleton exists.

Congenital hypoparathyroidism has also been reported in association with other anomalies, including the HDR (hypoparathyroidism, sensorineural deafness, and renal dysplasia) syndrome caused by heterozygous abnormalities in the gene encoding the transcription factor GATA3 (36) and a spectrum of phenotypes in patients that are hemizygous for a 1.5–3.0 Mb region of 22 q11.2 (37). The spectrum of the 22 q11.2 deletion phenotype includes DiGeorge syndrome (38) (hypoparathyroidism, typical facial features, cardiac lesions, and absent thymus), velocardiofacial syndrome (VCFS), conotruncal anomaly face syndrome, and some patients with Opitz syndrome (39). Recently, haploinsufficiency of the *TBX1* gene has been implicated in the molecular etiology of VCFS/DiGeorge syndrome (40). Whether athymia in DiGeorge syndrome contributes to the hypoparathyroid state remains to be determined. The skeletal sequelae of congenital hypoparathyroidism have not been described in neonates in these complex developmental syndromes either, but it would be difficult to distinguish the PTH-deficient skeletal consequences from dysmorphology associated with other elements of these syndromes.

Our studies describing the skeletal alterations in neonatal mice with hypoparathyroidism are therefore novel and indicate that a distinct neonatal skeletal phenotype occurs due to PTH deficiency that may not be remediable in the neonate with calcium or vitamin D treatment. Nevertheless, PTH deficiency in the fetus appears to retard trabecular bone development rather than completely inhibit it, inasmuch as *PTH*$^{-/-}$ mice in the postnatal state have increased rather than decreased metaphyseal trabecular bone (9). The signal for stimulating metaphyseal osteoblasts in the postnatal state could be PTHrP acting in a paracrine manner after release from differentiating osteoblasts or from other neighboring cells. In support of this are our previous observations in vivo that mice heterozygous for *PTHrP* gene ablation develop reduced trabecular bone volume in the postnatal stage (41) and that PTHrP can stimulate osteoblastic proliferation in vitro (42).

Although many of the molecular relationships with other regulators of skeletal development remain to be determined, our studies have clearly demonstrated a unique role for PTH in skeletal development in utero that complements the critical action that has been documented for PTHrP. Our observations may also be relevant to the "anabolic" effects of PTH in the postnatal state. Thus, intermittent exogenous PTH might recreate the effects of PTH in the fetus to enhance recruitment, commitment, and/or proliferation of osteoblast progenitors, as well as inhibit apoptosis of cells of the osteoblast lineage. Knowledge of these mechanisms may provide new targets for development of inducers of bone formation.

Acknowledgments

This work was supported by grants to A.C. Karaplis and D. Goltzman from the Medical Research Council of

Canada/Canadian Institutes of Health Research (MRC/CIHR), the National Cancer Institute of Canada, and the Canadian Arthritis Network. D. Miao and A.C. Karaplis are recipients of Fellowship and Scientist Awards, respectively, from MRC/CIHR.

1. Rodan, G.A., and Martin, T.J. 2000. Therapeutic approaches to bone diseases. *Science.* **289**:1508–1514.
2. Stewart, A.F., et al. 2000. Six-month daily administration of parathyroid hormone and parathyroid hormone-related protein peptides to adult ovariectomized rats markedly enhances bone mass and biomechanical properties: a comparison of human parathyroid hormone 1-34, parathyroid hormone-related protein 1-36, and SDZ-parathyroid hormone 893. *J. Bone Miner. Res.* **15**:1517–1525.
3. Dempster, D.W., et al. 2001. Effects of daily treatment with parathyroid hormone on bone microarchitecture and turnover in patients with osteoporosis: a paired biopsy study. *J. Bone Miner. Res.* **16**:1846–1853.
4. Neer, R.M., et al. 2001. Effect of parathyroid hormone (1-34) on fractures and bone mineral density in postmenopausal women with osteoporosis. *N. Engl. J. Med.* **344**:1434–1441.
5. Olsen, B.R., Reginato, A.M., and Wang, W. 2000. Bone development. *Annu. Rev. Cell Dev. Biol.* **16**:191–220.
6. Amizuka, N., Warshawsky, H., Henderson, J.E., Goltzman, D., and Karaplis, A.C. 1994. Parathyroid hormone-related peptide-depleted mice show abnormal epiphyseal cartilage development and altered endochondral bone formation. *J. Cell Biol.* **126**:1611–1623.
7. Vortkamp, A., et al. 1996. Regulation of rate of cartilage differentiation by Indian hedgehog and PTH-related protein. *Science.* **273**:613–622.
8. Lanske, B., et al. 1999. Ablation of the PTHrP gene or the PTH/PTHrP receptor gene leads to distinct abnormalities in bone development. *J. Clin. Invest.* **104**:399–407.
9. Miao, D., He, B., Goltzman, D., and Karaplis, A.C. 2001. Targeted disruption of PTH gene leads to abnormalities in skeletal development and calcium homeostasis. *J. Bone Miner. Res.* **16**:S161. (Abstr.)
10. Karaplis, A.C., et al. 1994. Lethal skeletal dysplasia from targeted disruption of the parathyroid hormone-related peptide gene. *Genes Dev.* **8**:277–289.
11. Silver, J., Naveh-Many, T., and Kronenberg, H.M. 2002. Parathyroid hormone molecular biology. In *Principles of Bone Biology*. 2nd edition. J.P. Bilezikian, L.G. Raisz, and G.A. Rodan, editors. Academic Press. San Diego, California, USA. 407–422.
12. Tybulewicz, V.L., Crawford, C.E., Jackson, P.K., Bronson, R.T., and Mulligan, R.C. 1991. Neonatal lethality and lymphopenia in mice with a homozygous disruption of the c-abl proto-oncogene. *Cell.* **65**:1153–1163.
13. Parr, B.A., and McMahon, A.P. 1995. Dorsalizing signal Wnt-7a required for normal polarity of D-V and A-P axes of mouse limb. *Nature.* **374**:350–353.
14. He, B., et al. 2001. Tissue-specific targeting of the pthrp gene: the generation of mice with floxed alleles. *Endocrinology.* **142**:2070–2077.
15. Miao, D., et al. 2001. Osteomalacia in hyp mice is associated with abnormal phex expression and with altered bone matrix protein expression and deposition. *Endocrinology.* **142**:926–939.
16. Panda, D.K., et al. 2001. Targeted ablation of the 25-hydroxyvitamin D 1 alpha-hydroxylase enzyme: evidence for skeletal, reproductive, and immune dysfunction. *Proc. Natl. Acad. Sci. USA.* **98**:7498–7503.
17. Brown, E.M. 2000. G protein-coupled, extracellular Ca2+ (Ca2+(o))-sensing receptor enables Ca2+(o) to function as a versatile extracellular first messenger. *Cell Biochem. Biophys.* **33**:63–95.
18. Kovacs, C.S., et al. 1998. Regulation of murine fetal-placental calcium metabolism by the calcium-sensing receptor. *J. Clin. Invest.* **101**:2812–2820.
19. Kovacs, C.S., Chafe, L.L., Fudge, N.J., Friel, J.K., and Manley, N.R. 2001. Pth regulates fetal blood calcium and skeletal mineralization independently of pthrp. *Endocrinology.* **142**:4983–4993.
20. Amizuka, N., et al. 1996. Programmed cell death of chondrocytes and aberrant chondrogenesis in mice homozygous for parathyroid hormone-related peptide gene deletion. *Endocrinology.* **137**:5055–5067.
21. Amling, M., et al. 1997. Bcl-2 lies downstream of parathyroid hormone-related peptide in a signaling pathway that regulates chondrocyte maturation during skeletal development. *J. Cell Biol.* **136**:205–213.
22. Gerber, H.P., et al. 1999. VEGF couples hypertrophic cartilage remodeling, ossification and angiogenesis during endochondral bone formation. *Nat. Med.* **5**:623–628.
23. Hanahan, D. 1997. Signaling vascular morphogenesis and maintenance. *Science.* **277**:48–50.
24. Aguirre, J., et al. 2001. Endothelial nitric oxide synthase gene-deficient mice demonstrate marked retardation in postnatal bone formation, reduced bone volume, and defects in osteoblast maturation and activity. *Am. J. Pathol.* **158**:247–257.
25. Kaufman, M.H. 1992. *The atlas of mouse development*. Academic Press. San Diego, California, USA. 219–290.
26. Calvi, L.M., et al. 2001. Activated parathyroid hormone/parathyroid hormone-related protein receptor in osteoblastic cells differentially affects cortical and trabecular bone. *J. Clin. Invest.* **107**:277–286.
27. Jilka, R.L., et al. 1999. Increased bone formation by prevention of osteoblast apoptosis with parathyroid hormone. *J. Clin. Invest.* **104**:439–446.
28. Hock, J.M., et al. 2001. Osteoblast apoptosis and bone turnover. *J. Bone Miner. Res.* **16**:975–984.
29. Ahn, T.G., Antonarakis, S.E., Kronenberg, H.M., Igarashi, T., and Levine, M.A. 1986. Familial isolated hypoparathyroidism: a molecular genetic analysis of 8 families with 23 affected persons. *Medicine (Baltimore).* **65**:73–81.
30. Arnold, A., et al. 1990. Mutation of the signal peptide-encoding region of the preproparathyroid hormone gene in familial isolated hypoparathyroidism. *J. Clin. Invest.* **86**:1084–1087.
31. Parkinson, D.B., Thakker, R.V. 1992. A donor splice site mutation in the parathyroid hormone gene is associated with autosomal recessive hypoparathyroidism. *Nat. Genet.* **1**:149–152.
32. Sunthornthepvarakul, T., Churesigaew, S., and Ngowngarmratana, S. 1999. A novel mutation of the signal peptide of the preproparathyroid hormone gene associated with autosomal recessive familial isolated hypoparathyroidism. *J. Clin. Endocrinol. Metab.* **84**:3792–3796.
33. Pearce, S.H., et al. 1996. A familial syndrome of hypocalcemia with hypercalciuria due to mutations in the calcium-sensing receptor. *N. Engl. J. Med.* **335**:1115–1122.
34. Ding, C., Buckingham, B., and Levine, M.A. 2001. Familial isolated hypoparathyroidism caused by a mutation in the gene for the transcription factor GCMB. *J. Clin. Invest.* **108**:1215–1220.
35. Gunther, T., et al. 2000. Genetic ablation of parathyroid glands reveals another source of parathyroid hormone. *Nature.* **406**:199–203.
36. Muroya, K., et al. 2001. GATA3 abnormalities and the phenotypic spectrum of HDR syndrome. *J. Med. Genet.* **38**:374–380.
37. Greig, F., Paul, E., DiMartino-Nardi, J., Saenger, P. 1996. Transient congenital hypoparathyroidism: resolution and recurrence in chromosome 22q11 deletion. *J. Pediatr.* **128**:563–567.
38. Hur, H., Kim, Y.J., Noh, C.I., Seo, J.W., Kim, M.H. 1999. Molecular genetic analysis of the DiGeorge syndrome among Korean patients with congenital heart disease. *Mol. Cells.* **9**:72–77.
39. Weinzimer, S.A. 2001. Endocrine aspects of the 22q11.2 deletion syndrome. *Genet. Med.* **3**:19–22.
40. Merscher, S., et al. 2001. TBX1 is responsible for cardiovascular defects in velo-cardio-facial/DiGeorge syndrome. *Cell.* **104**:619–629.
41. Amizuka, N., et al. 1996. Haploinsufficiency of parathyroid hormone-related peptide (PTHrP) results in abnormal postnatal bone development. *Dev. Biol.* **175**:166–176.
42. Miao, D., et al. 2001. Parathyroid hormone-related peptide stimulates osteogenic cell proliferation through protein kinase C activation of the Ras/mitogen-activated protein kinase signaling pathway. *J. Biol. Chem.* **276**:32204–32213.